Atmospheric Environment 266 (2021) 118691

Contents lists available at ScienceDirect

Atmospheric Environment

journal homepage: www.elsevier.com/locate/atmosenv

A study of the nitrogen and phosphorus imbalance in East Asia based on the distribution patterns of and stoichiometric variation in global atmospheric nitrogen and phosphorus

Hung-Yu Chen [a,*], Li-Min Huang [a], Tung-Yuan Ho [b], Kuo-Ping Chiang [c], Wen-Chen Chou [c]

[a] Department of Marine Environmental Informatics, National Taiwan Ocean University, Keelung, 202, Taiwan
[b] Research Center for Environmental Changes, Academia Sinica, Taipei, 115, Taiwan
[c] Institute of Marine Environment and Ecology, National Taiwan Ocean University, Keelung, 202, Taiwan

ARTICLE INFO

Keywords:
Atmospheric deposition
Nitrogen species
Phosphorus species
Nitrogen-to-phosphorus ratio
Nutrient imbalance

ABSTRACT

To explore nitrogen (N) and phosphorus (P) imbalances in the atmosphere in East Asia, we set up an atmospheric sampling station at the southern end of the East China Sea. From April 2019 to March 2020, we collected atmospheric particulates and rainwater samples and performed chemical analyses of inorganic and organic N and P species in the samples. In this study, the average N/P ratio of dry deposition was 443 ± 366, and it was affected mainly by changes in the wind direction in different seasons. The average N/P ratio of wet deposition was 333 ± 362, and the distribution of the ratio was affected mainly by rainfall.

In addition, this study categorized the global N and P fluxes into four distribution patterns: high N and high P (HNHP), high N and low P (HNLP), low N and high P (LNHP), and low N and low P (LNLP). The Galloway/Mahowald ratio (G/M ratio) ranges and distribution areas of these four types are 450–2200 (Western Europe, southeastern South America), 660–4400 (East Asia, North America), 0.2–200 (Southern Europe, North Africa) and 45–450 (South Asia). Among them, mainland China in East Asia (HNLP) usually has a higher G/M ratio. The study area has the same characteristics as most HNLP regions (coastal China and the southeastern coast of North America). This study also highlights the imbalance in the ratio of N to P caused by excessive active N emissions from human activities.

1. Introduction

Due to the rapid development of industry and agriculture, the combustion and emissions of fossil fuels and biomass fuels have increased, as has the production of a large amount of chemical fertilizers; these factors have resulted in an increase in the concentrations of nitrogen (N) and phosphorus (P) in the atmosphere (Spokes et al., 2006). Fowler et al. (2013) pointed out that anthropogenic N emission (210 Tg N yr^{-1}) in 2010 exceeded natural emissions (203 Tg N yr^{-1}). Moreover, anthropogenic P emissions before the Industrial Revolution were approximately >15 Mt P yr-1, and by 2000, they were >30 Mt P yr^{-1}, representing an approximately twofold increase (Smil, 2000). The significant increase in N and P emissions to the atmosphere from human activities (especially in East Asia) has already affected biogeochemical cycles in marginal seas (Chen and Chen, 2008). This phenomenon will lead to worsening marine ecological environmental problems, such as eutrophication and red tides, and changes in the structure of aquatic communities (Yu et al., 2020).

Galloway et al. (2008) developed a global model of total atmospheric N deposition fluxes and noted that the fluxes in different regions worldwide are, in descending order, those of East Asia (600–6000 mg N $m^{-2}yr^{-1}$), Europe (300–3000 mg N $m^{-2}yr^{-1}$), North America (300–2000 mg N $m^{-2}yr^{-1}$), Central and South America (100–1000 mg N $m^{-2}yr^{-1}$), Southeast Asia (100–1000 mg N $m^{-2}yr^{-1}$), and North Africa (50–500 mg N $m^{-2}yr^{-1}$). Furthermore, a global model of total atmospheric total P fluxes (Mahowald et al., 2008) demonstrated that North Africa (Sahara Desert) has the highest flux, of approximately 50–500 mg P $m^{-2}yr^{-1}$, followed by 5–100 mg P $m^{-2}yr^{-1}$ in Europe, 2–50 mg P $m^{-2}yr^{-1}$ in Central and South America, 2–10 mg P $m^{-2}yr^{-1}$ in East Asia, and 0.5–5 mg P $m^{-2}yr^{-1}$ in North America and Southeast Asia.

Liebig's law of the minimum indicates that in ecosystems, the growth of organisms is controlled not by the total nutrient availability but by the

* Corresponding author.
E-mail address: hychen@mail.ntou.edu.tw (H.-Y. Chen).

https://doi.org/10.1016/j.atmosenv.2021.118691
Received 26 May 2021; Received in revised form 19 August 2021; Accepted 20 August 2021
Available online 24 August 2021

scarcest nutrient or the limiting nutrient (De Baar, 1994). In ecosystems, the nitrogen-to-phosphorus ratio affects the composition of the biological community. The amount of biological N fixation in the soil will decrease with the increase in the nitrogen-to-phosphorus ratio (Chen et al., 2016). The same phenomenon is also found in aquatic ecosystems (Mills et al., 2004). In marine environments, a nitrogen-to-phosphorus ratio (N/P ratio) of 16 (the Redfield ratio) is the most suitable for most phytoplankton growth. External nutrient supplies are very important for the growth of organisms (Chen and Huang, 2018); they may increase the productivity of the ecosystem or may cause some organisms to overproduce and damage the environment. Therefore, it is very important to determine the limiting nutrients in ecosystems. Through the evaluation of limiting nutrients, we can better understand the ecological conditions of various regions. This is the main reason why research on the topic of nutrient limitation has become more common (Elser et al., 2007).

The Redfield ratio or Redfield stoichiometry refers mainly to the consistency of carbon, N and P ratios between ocean chemistry and biochemistry. When nutrients are not limited, the Redfield proportion is 106C: 16N: 1P (Garcia et al., 2018). However, if the nutrients in seawater are limited, the growth of organisms in seawater will be further affected, and the productivity of seawater will also be affected. In oligotrophic oceans, the bioavailable forms of P are severely depleted along with N, which causes P stress in plankton. The addition of P usually does not lead to an increase in autotrophic activity or biomass. Therefore, it is necessary to confirm the oligotrophic conditions in the affected area, which could be N limitation or NP colimitation (Moore et al., 2013).

Atmospheric deposition provides nutrients such as N and P to coastal areas; it can increase ocean productivity by 8% and even maintains approximately 10% of primary production in tropical areas in the western Pacific (Martino et al., 2014; Mackey et al., 2012; Xing et al., 2018). In Europe, the atmospheric nutrient supply equals or exceeds riverine inputs in some areas (Spokes et al., 2006). In the seas of East Asia, the percentage of the total productivity attributed to the atmospheric nutrient supply is 0.3–6.7% in the Yellow Sea (Qi et al., 2020), 12–14% in the southern Sea of Japan (Yan and Kim, 2015), 8.2% in the southern East China Sea (Chen et al., 2010) and 5.6–8.7% in the northern South China Sea (Chen and Huang, 2018). Therefore, the contributions from human activities in East Asia have a great impact on the atmospheric nutrient supply, which in turn affects the nutrient balance in marine ecosystems (Yu et al., 2020).

P in the atmosphere comes mainly from natural sources (deserts, etc.), and P emissions are significantly lower than human-based N emissions; as a result, the atmospheric N/P ratio is generally higher than the Redfield ratio. For example, the North Atlantic Ocean and the East China Sea are both clearly P-limited areas, while only a few areas worldwide, such as Singapore and the Mediterranean region (Sahara Desert), are N-limited areas (Baker et al., 2003; He et al., 2011; Moore et al., 2013). Moore et al. (2013) pointed out that the N/P ratio in the global atmosphere was approximately 62 before 1860 and reached 228 by 2000. Unlike the relatively stable N/P ratio in rivers (44–33), the N/P ratio in the atmosphere fluctuates greatly. The main reason for this is that anthropogenically active N emissions have increased by three times since 1860. It is estimated that N emissions will increase by an additional 10–20% by 2050. Therefore, the atmospheric N/P ratio in the future will be different from the current atmospheric N/P ratio.

The Redfield ratio has been widely utilized as an important indicator of limiting factors in the marine biogeochemical cycle, and the atmosphere generally has high N/P ratios. However, related studies in the past have rarely discussed N/P ratios in the global atmosphere. Therefore, this study will use the flux models of Galloway et al. (2008) and Mahowald et al. (2008) to characterize global N and P flux distribution patterns and then calculate the Galloway/Mahowald flux ratio (G/M ratio) in order to discuss the phenomenon of global and regional atmospheric N/P ratio imbalances.

2. Methodology

2.1. Sampling

The atmospheric sampling station used in this study is located on the Matsu Islands (26.167°N, 119.917°E) at the mouth of the Min River, adjacent to the mainland to the west (approximately 97 km) and the Taiwan Strait to the east, approximately 220 km from Taiwan (Fig. 1). The sampling site is approximately 10 m from the coastline and approximately 10 m above sea level to avoid interference from human influences. The dry and wet deposition sampling period in this study was from April 2019 to March 2020 (12 months). The climate of the study area is a subtropical oceanic climate. The sampling area is affected mainly by the northeast monsoon from winter to the following spring and the southwest monsoon in summer and autumn. The main rainy season is from April to September in each year, and the annual rainfall is approximately 1000 mm.

A high-volume air sampling system (TE-5170; TISCH) was used to collect size-segregated particulate aerosols via a five-stage particle size fractionator (cascade impactor, CI; TE-3000, TISCH). Particulate aerosol samples were collected using a high-volume system fitted with slotted CI quartz fiber filters (TE-230-QZ, TISCH; 146 × 153 mm); the impactors had cutoff diameters equivalent to 50% efficiency and were used for the collection of size-fractionated particles as follows: stage 1 (>7.2 μm), stage 2 (3.0–7.2 μm), stage 3 (1.5–3.0 μm), stage 4 (0.95–1.5 μm), and stage 5 (0.49–0.95 μm). Particles that passed through the CI were trapped on a backup filter (<0.49 μm). Prior to use, the filters were heated in an oven at 550 °C for 3 h. The flow rate was set to 0.85 m^3 min^{-1}, and the total sampling time was 168 h, yielding a total sampled air volume of approximately 9,000 m^3. Over the sampling period 12 sets of size segregated particulate aerosol samples (a total of 72 individual size samples) were collected. The filter samples were stored at −24 °C until analysis. Each filter obtained from aerosol sampling was extracted by sonication with 200 W output power (DC200H; Delta Electronics, Inc., Taiwan) for 3 h in 100 mL of Milli-Q water (>18 MΩ cm). After extraction, the extract will be immediately analyzed for various chemical species. Full details of the dry deposition sampling and extraction procedures have been described by Chen et al. (2010).

The wet deposition sample collectors were made of stainless steel catchment funnels (27 cm in diameter) and clean 5-L brown glass bottles. Samples that contained less than 500 mL of rainwater were excluded from the study because the amount was insufficient for the experiments and analysis. Samples were collected daily from April 3, 2019, to March 28, 2020 and a total of 53 wet deposition samples were collected. The rainwater samples were initially filtered using a preashed

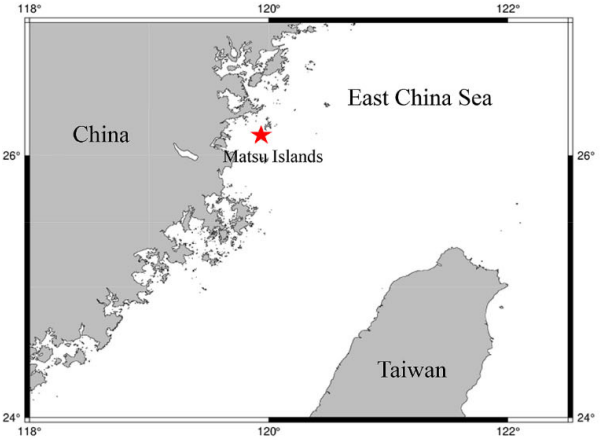

Fig. 1. Sampling location.

quartz fiber membrane (20 mm, Millipore). The filtered samples were then poured into brown glass bottles that were sealed with Parafilm before being stored in a refrigerator at 4 °C. Full details of the wet deposition sampling procedures are described in Chen et al. (2015).

2.2. Chemical analysis

For the analysis of N and P species, aerosol extracts or rainwater samples were diluted to an appropriate concentration and analyzed using colorimetric methods. The concentrations of ammonium (NH_4^+) and nitrite (NO_2^-) ions were determined by the indophenol blue (Pai et al., 2001) and pink azo dye (Pai and Yang, 1990) colorimetric methods, respectively. The concentration of nitrate ions (NO_3^-) was determined by flow-injection analysis using an online cadmium reductor. The NO_3^- in the rainwater or aerosol extract was reduced to NO_2^- using a cadmium–copper tube before the NO_2^- concentration was measured. The NO_2^- concentration was subsequently used to calculate the NO_3^- concentration (Pai and Riley, 1994). The P content of the filtered extracts or rainwater was measured using a double-beam spectrophotometer (SP8001, Metertech); similarly, the phosphate content was measured with a 5 cm quartz cell using the molybdate blue method (Murphy and Riley, 1962; Pai et al., 1990). The results of the blank tests (n = 12) in dry deposition (concentration in nmol per filter) and wet deposition (concentration in μM) were NH_4^+ (1.42 ± 0.19 and 0.88 ± 0.31), NO_2^- (1.80 ± 0.10 and 0.03 ± 0.01), NO_3^- (2.09 ± 0.51 and 0.50 ± 0.15) and PO_4^{3-} (0.23 ± 0.008 and 0.028 ± 0.004). The limit of detection (LOD) was calculated using 3δ of the blank. The results of LOD in dry deposition (concentration in nmol m^{-3} which was calculated with 4000 m^3 of sampling volume) and wet deposition (concentration in μM) were NH_4^+ (0.050 and 0.70), NO_2^- (0.022 and 0.02), NO_3^- (0.140 and 0.45) and PO_4^{3-} (0.003 and 0.012). All samples had measured concentrations at least three times greater than the blank measurements.

In the present study, we define both water-soluble inorganic N (WSIN) and dissolved inorganic N (DIN) as the sum of NH_4^+, NO_2^-, and NO_3^-, and water-soluble inorganic P (WSIP) and dissolved inorganic P (DIP) are defined as the concentration of PO_4^{3-}. Both organic N (ON) and organic P (OP) have complex compositions in the environment. Therefore, the aerosol extract or rainwater oxidized all the N (TN) or P (TP) species into NO_3^- or PO_4^{3-}, respectively. The digestion reagents for TN and TP included 2 mL of different concentrations of persulfate oxidation (PO); the concentration for N was 0.037 M, and that for P was 0.185. The digestion methods were ultraviolet (UV) light illumination and a digestion bomb for TN and TP, respectively. Ethylene diamine tetraacetic acid (EDTA), quinolone, and urea were employed as the standards for the UV oxidation method for TN. Sodium tripolyphosphate (STP) and tetrasodium pyrophosphate (TSS) were used to confirm the oxidation efficiency of the digestion bomb for TP. The oxidation efficiencies were 102 ± 4%, 92 ± 5%, 100 ± 6%, 95 ± 3% and 103 ± 3% for EDTA, quinolone, urea, STP and TSS, respectively. The ON or OP concentration was obtained by subtracting the IN or IP concentration from the TN or TP concentration, respectively. The following equations were used to calculate the concentrations (nmol m^{-3} and μM and for dry and wet deposition, respectively) of these N and P species:

$$[IN] = [NH_4^+] + [NO_2^-] + [NO_3^-] \quad (1)$$

$$[ON] = [TN] - [IN] \quad (2)$$

$$[IP] = [PO_4^{3-}] \quad (3)$$

$$[OP] = [TP] - [IP] \quad (4)$$

Full details of the N and P analysis have been described in Chen and Huang (2020) and Huang and Zhang (2009), respectively.

2.3. Flux estimation of dry and wet deposition and calculation of G/M ratio

The equation used for the dry deposition flux calculations is as follows:

$$F_d = C_d \times V_d \quad (5)$$

where F_d is the dry deposition flux (mmol m^{-2} yr^{-1}), C_d is the species concentration (nmol m^{-3}), and V_d is the aerosol deposition velocity (cm s^{-1}). The deposition velocity for coarse-particle aerosols is set as 2.0 cm s^{-1}, whereas that for fine-particle aerosols is 0.1 cm s^{-1} (Chen and Huang, 2020).

This study applies the N species wet deposition flux estimation method of Zhang et al. (2019), and the calculation method is as follows:

$$F_w = C_m \times I \quad (6)$$

where F_w is the wet deposition flux (mmol m^{-2} yr^{-1}), C_m is the species concentration (μM), and I is the accumulated rainfall (mm).

Since the measured data for the concentrations of the global atmospheric deposition of N and P are not complete, this study uses the atmospheric deposition N and P flux models proposed by Galloway et al. (2008) and Mahowald et al. (2008), respectively, to calculate the G/M ratio (molar ratio). The ratio is calculated as follows:

$$\frac{G}{M} = \frac{Galloway's\ nitrogen\ flux}{Mahowald's\ phosphorus\ flux} \quad (7)$$

3. Results and discussion

3.1. Dry deposition

The concentrations of N species in atmospheric dry deposition in this study area exhibit obvious seasonal changes (Table 1). The average concentration of WSTN is 209 ± 66 nmol m^{-3}, with a maximum of 345 nmol m^{-3} in January and a minimum of 85.9 nmol m^{-3} in July (Fig. 2). The difference between the highest and lowest concentrations is approximately 4 times. The main reason for the concentration changes is the difference in the sources of air masses brought by the monsoon (Fig. 3). The average concentration of WSTN in this study is higher than that in other regions at similar latitudes such as the eastern Mediterranean (Turkey) (63.5 nmol m^{-3}, Nehir and Koçak, 2018), the southwestern North Atlantic (Miami) (53.4 nmol m^{-3}) and Barbados (21.2 nmol m^{-3}, Zamora et al., 2013). It is also higher than the 52.1 nmol m^{-3} (Wu et al., 2018) value obtained in the northern South China Sea (Daya Bay) and the 120 nmol m^{-3} value obtained in the South China Sea (He et al., 2011). However, the concentration of WSTN in the atmosphere in this region is significantly lower than the 945 nmol m^{-3} (Yu et al., 2020) measured in Qinhuangdao the and 1196 nmol m^{-3} measured in Jiaozhou Bay in northern China (Xing et al., 2018). Therefore, the atmosphere in East Asia is affected by high anthropogenic N emissions, and the northern part of East Asia (especially northern China) has extremely high WSTN concentrations. However, the concentration tends to decrease towards the southern part of East Asia (Chen and Huang, 2018).

In this study area, the concentration of water-soluble inorganic N (WSIN) in the dry deposition is 157 ± 57 nmol m^{-3} (accounting for 75% of WSTN), and the water-soluble organic N (WSON) concentration is 52.3 ± 18.9 nmol m^{-3} (accounting for 25% of WSTN). The average concentration of WSIN in dry deposition in this study area is greater than that of WSON, and the ratio of WSIN to WSON is approximately 3:1. This ratio is lower than the 4:1 ratio calculated for Qinhuangdao (Yu et al., 2020) and the 5:1 ratio measured calculated for Jiaozhou Bay (Xing et al., 2018) in the Yellow Sea.

In this study, (Fig. 4), the average concentration of WSTP in the dry deposition is 0.51 ± 0.32 nmol m^{-3}, which is lower than the

Table 1
Monthly average concentrations of nitrogen and phosphorus species in dry deposition (nmol m^{-3}).

	WSTN	WSON	WSIN	NH_4^+	NO_3^-	WSTP	WSOP	WSIP
Apr-19	251.3	53.9	197.3	115.7	81.2	1.05	0.38	0.66
May-19	223.7	39.3	184.5	115.2	68.6	0.44	0.19	0.26
Jun-19	173.0	44.3	128.6	72.7	55.4	0.50	0.35	0.15
Jul-19	85.6	21.7	64.2	36.5	27.4	0.23	0.14	0.09
Aug-19	152.9	47.4	105.5	54.4	50.8	0.87	0.11	0.76
Sep-19	137.2	27.6	109.6	61.8	47.0	0.97	0.26	0.71
Oct-19	226.3	96.3	130.0	70.9	58.5	0.89	0.14	0.75
Nov-19	172.6	52.6	120.0	61.1	58.5	0.32	0.08	0.24
Dec-19	215.6	50.4	165.3	89.1	75.6	0.25	0.11	0.14
Jan-20	345.1	58.4	286.7	171.7	113.6	0.27	0.06	0.22
Feb-20	246.8	65.1	181.7	117.7	62.9	0.16	0.04	0.12
Mar-20	276.0	70.4	205.7	103.3	101.4	0.21	0.06	0.16
Mean	208.9 ± 66.4	52.3 ± 18.9	156.6 ± 56.8	89.2 ± 35.8	66.7 ± 22.6	0.51 ± 0.32	0.16 ± 0.10	0.35 ± 0.26

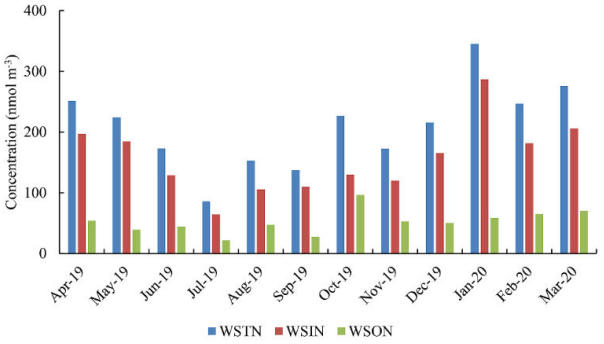

Fig. 2. Variations in monthly average concentrations of WSTN, WSIN and WSON in dry deposition.

1.24 nmol m^{-3} measured in Jiaozhou Bay (Xing et al., 2018), the 2.35 nmol m^{-3} in measured Qinhuangdao (Yu et al., 2020) and the 12.5 nmol m^{-3} measured in Singapore (He et al., 2011). The distributions of the concentrations of N and P species in dry deposition are different, and they do not exhibit clear seasonal changes. It is speculated that the study area may lack a supply of dust particles, resulting in a low WSTP concentration. The average concentration of WSIP is 0.35 ± 0.27 nmol m^{-3} (accounting for 69% of WSTP), and the monthly average concentration of WSOP is 0.16 ± 0.1 nmol m^{-3} (accounting for 31% of WSTP). The distributions of WSIP and WSOP are similar to that of WSTP. In this area, the N and P species in dry atmospheric deposition are mainly inorganic. The WSIP concentration is higher than the WSOP concentration in the study period except in the summer, when the WSOP concentration is higher due to inputs of P originating from the sea.

3.2. Wet deposition

Table 2 presents the monthly average concentration of total dissolved N (TDN) in wet deposition. The monthly average concentration of TDN (Fig. 5) is 115 ± 58 μM; the maximum TDN concentration occurs in October (252 μM) and the minimum occurs in July (42 μM). The difference between the highest concentration and the lowest concentration is approximately 6 times. The concentration of TDN is also affected by seasonal changes. In summer, the main source of air masses is the southern ocean; in contrast, in the other months, the main source of air masses is the northern continent. In addition, during the rainy season in summer in the sampling area, high rainfall will also dilute the TDN concentration, resulting in its minimum summer value. The average concentration of TDN in this study area is lower than the 225 μM measured in Jiaozhou Bay (Xing et al., 2017) and the 160 μM measured in Keelung (Chen et al., 2015). In Northeast Asia, due to the influence of human activities, the TDN concentration in wet deposition is generally greater than 100 μM. In other regions that are relatively unaffected by human activities, such as the eastern Mediterranean (24 μM) and Australia (18 μM), the concentration of TDN is far below 100 μM.

The average concentration of DIN (dissolved inorganic N) in wet precipitation is 91.4 ± 44.7 μM (79% of TDN), and the average concentration of DON (dissolved organic N) is 24.7 ± 16.7 μM (21% of TDN). Similar to those of TDN, the highest concentration of DIN occurs in October (187 μM), and the lowest concentration occurs in July (38 μM). The N species in both wet and dry deposition were mainly inorganic. The average concentration of DIN in this study was similar to a previous DIN value (102 μM) measured at the southern end of the East China Sea (Chen et al., 2015); however, the average concentration of DON in this study is only half of the concentration measured in the southern East China Sea (57 μM). The ratio of inorganic N to organic N in this study area is 4:1, which is higher than the 2:1 ratio calculated for the southern East China Sea (Chen et al., 2015). This may be because this sampling site is located closer to the mainland, resulting in a significantly higher proportion of inorganic N (79%) at the sampling site than in the southern East China Sea (64%).

The average monthly concentration of total dissolved P (TDP; Fig. 6) in wet deposition is 0.48 ± 0.27 μM; the highest concentration occurs in December (1.08 μM), and the lowest concentration (0.18 μM) occurs in May. The difference between the highest monthly average concentration and the lowest monthly average concentration is 6 times. The TDP concentration in the study area is approximately half of the 0.84 μM value measured in the Yellow Sea (Jiaozhou Bay) (Xing et al., 2017) and the 0.84 μM measured in Singapore (He et al., 2011). However, it is still higher than the 0.13 μM value measured in the Baltic Sea (Rolff et al., 2008). Therefore, the global variations in TDP concentrations are obviously affected by the intensity of human activities.

The average concentration of DIP (dissolved inorganic P) is 0.28 ± 0.20 μM (57% of TDP). Similar to those of TDP, the highest concentration occurs in December (0.79 μM), and the lowest concentration occurs in May (0.1 μM). Although the P species in wet precipitation are mainly inorganic, the proportion of organic P in wet precipitation (43%) is higher than that in dry precipitation (31%). The higher ratio of organic P in wet deposition may be due to the different source compositions of organic and inorganic P. The distributions of the DIP and DOP concentrations are roughly the same as that of TDP. Both have the highest concentration in winter and the lowest concentration in May. DIP and DOP are also strongly correlated (r = 0.77). It is speculated that the two species may have the same main source.

Zamora et al. (2013) pointed out when the flux of WSTN is less than 10 mmol m^{-2} yr^{-1}, it usually indicates a low-pollution area, such as Barbados in the southwestern North Atlantic (8.9 ± 4.7 mmol m^{-2} yr^{-1}). A WSTN flux between 10 and 40 mmol m^{-2} yr^{-1} indicates a region with moderate anthropogenic influence, such as Kofu city in the southern part of the Sea of Japan (22.9 mmol m^{-2} yr^{-1}; Matsumoto et al., 2014) and

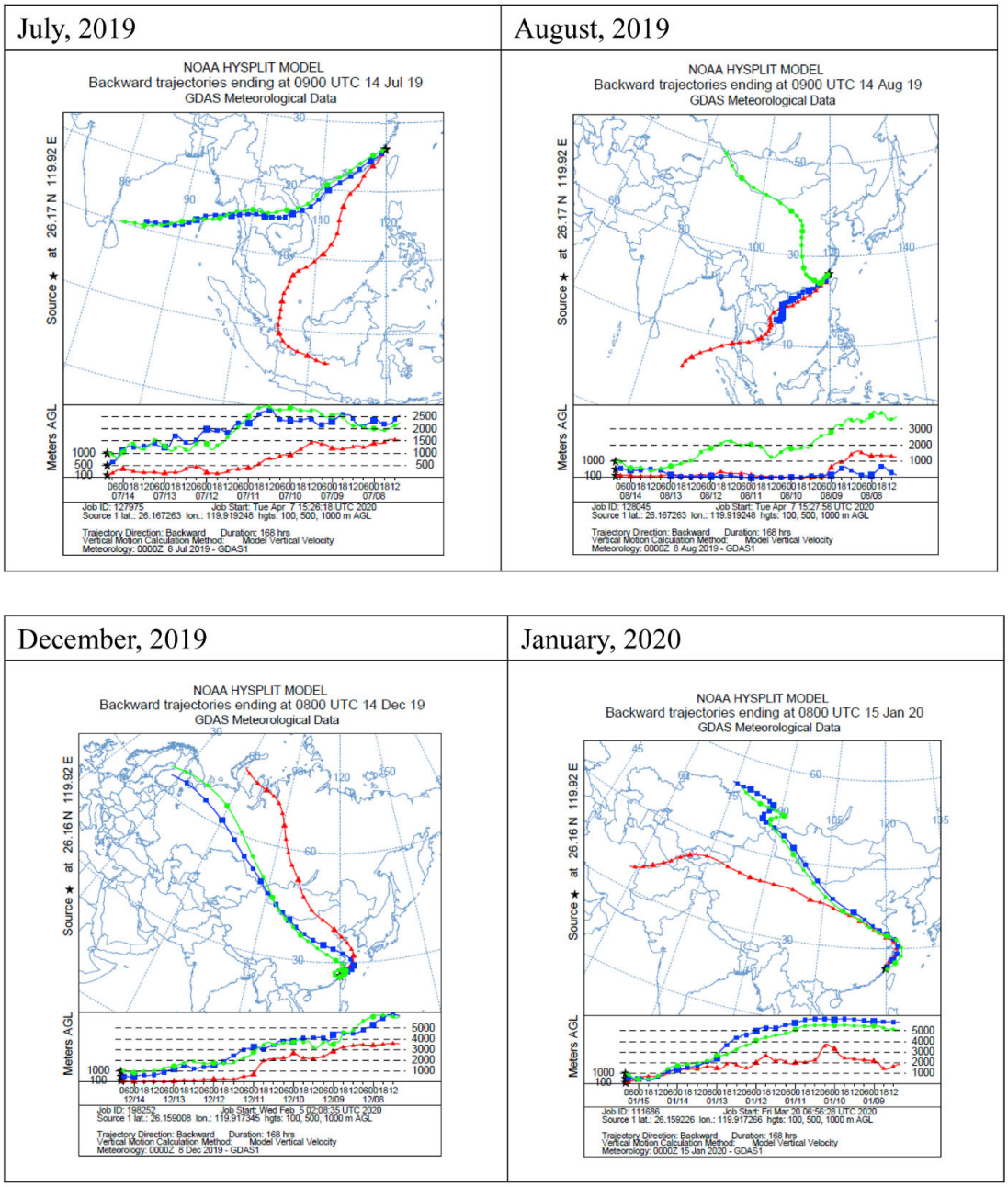

Fig. 3. The air-mass back trajectories for starting altitudes of 100,500, and 1000m above ground level calculated from the database of the National Ocean and Atmospheric Administration (NOAA) for the sampling period under the southwest monsoon (July and August 2019) and northeast monsoon (December 2019 and January 2020).

Turkey in the eastern Mediterranean (21.1 mmol m^{-2} yr^{-1}; Nehir and Koçak, 2018). A WSTN flux greater than 40 mmol m^{-2} yr^{-1} usually indicates an area that is seriously affected by anthropogenic emissions, such as those in East Asia. The geographical distribution of WSTN tends to decrease from the north (a densely populated area) to the south, such as from Jiaozhou Bay in the Yellow Sea (75.9 mmol m^{-2} yr^{-1}; Xing et al., 2018), to Keelung in the southern part of the East China Sea (61 mmol m^{-2} yr^{-1}; Chen et al., 2010) and Dongsha Island in the northern part of the South China Sea (50 ± 23 mmol m^{-2} yr^{-1}; Chen and Huang, 2018). The flux of WSTN in this study area is 41.9 ± 11.6 mmol m^{-2} yr^{-1} (Eq. (5)), indicating that this is an area with more serious human pollution; this value is similar to the fluxes in the East China Sea and South China Sea (Table 3).

Unlike that of N species, the main sources of P species in the atmosphere are generally related to crustal dust. When WSTP<0.5 mmol m^{-2} yr^{-1}, it indicates that the area is less affected by sand and dust, such as Miami (0.09 mmol m^{-2} yr^{-1}) and Barbados (0.10 mmol m^{-2} yr^{-1}) in the southwestern North Atlantic (Zamora et al.,

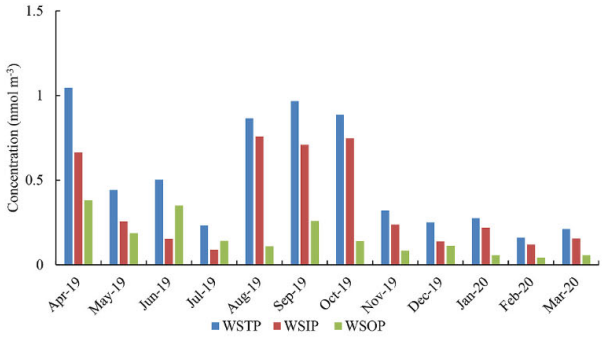

Fig. 4. Variations in monthly average concentrations of WSTP, WSIP and WSOP in dry deposition.

2013) and Jiaozhou Bay in the Yellow Sea (0.26 mmol m^{-2} yr^{-1}; Xing et al., 2018). Among them, although the Yellow Sea does not receive dust particles during nondust-storm periods, it is affected by human activities (biomass combustion, fossil combustion), resulting in its flux being 2–3 times that in the North Atlantic. A WSTP >0.5 mmol m^{-2} yr^{-1} indicates that the area is greatly affected by crustal dust. Among such areas, the Mediterranean region, such as the Levant Sea in southern Europe (0.80 mmol m^{-2} yr^{-1}; Carbo et al., 2005) and Crete (0.69 mmol m^{-2} yr^{-1}; Violaki et al., 2017) in the eastern Mediterranean, is affected mainly by the Sahara Desert. The northern part of China is affected by the Taklimakan Desert, which leads to extremely high P fluxes in the Yellow Sea during sandstorm periods (1.41 mmol m^{-2} yr^{-1}; Shi et al., 2013). The WSTP flux of 0.08 ± 0.05 mmol m^{-2} yr^{-1} (Eq. (5)) in the study area is < 0.500 mmol m^{-2} yr^{-1}. Since there were almost no dust events during the sampling period, the study area can be considered an area with low annual WSTP flux (Chen and Chen, 2008).

Wet deposition is affected by rainfall in different regions and at different times. It is difficult to understand its substantial impact on the environment by considering only changes in concentration, so it is necessary to estimate fluxes based on actual rainfall data (Chen et al., 2015). The annual flux of TDN is affected mainly by rainfall and human activities. The regions where the TDN flux is < 100 mmol m^{-2} yr^{-1} include Crete in the eastern Mediterranean (22 mmol m^{-2} yr^{-1}; annual rainfall of approximately 800 mm) (Violaki et al., 2010), Miami in the southwestern North Atlantic (29 mmol m^{-2} yr^{-1}; annual rainfall of approximately 1600 mm) (Zamora et al., 2013) and Puerto Rico (17 mmol m^{-2} yr^{-1}; annual rainfall of approximately 1400 mm) (Gioda et al., 2011). These areas also experience low rainfall. Areas in which the global TDN flux >100 mmol m^{-2} yr^{-1} include Keelung in the southern part of the East China Sea (327 mmol m^{-2} yr^{-1}; annual rainfall of approximately 3500 mm) (Chen et al., 2015) and Singapore (410 mmol m^{-2} yr^{-1}; annual rainfall of approximately 2200 mm) (He et al., 2011). These areas are all areas with relatively high annual rainfall (Table 3). Due to the influence of anthropogenic activities, Jiaozhou Bay in the Yellow Sea (196 mmol m^{-2} yr^{-1}; Xing et al., 2017) has a high TDN flux despite the annual rainfall being only 800 mm. The annual rainfall in the study area is only 1000 mm, and it is located a certain distance from the northern part of the mainland, so it is considered an area with low TDN flux (57.3 ± 11.3 mmol m^{-2} yr^{-1}; Eq. (6)).

The regions with low annual TDP flux (<0.5 mmol m^{-2} yr^{-1}) include Miami (0.09 mmol m^{-2} yr^{-1}) and Barbados (0.09 mmol m^{-2} yr^{-1}; Zamora et al., 2013) in the southwestern North Atlantic. The low TDP flux in these regions is due to the low rainfall. Areas with high annual TDP flux (>0.5 mmol m^{-2} yr^{-1}) are affected mostly by rainfall, human activities or crustal dust. These areas include Crete in the eastern Mediterranean (0.82 mmol m^{-2} yr^{-1}; Violaki et al., 2010), Jiaozhou Bay in

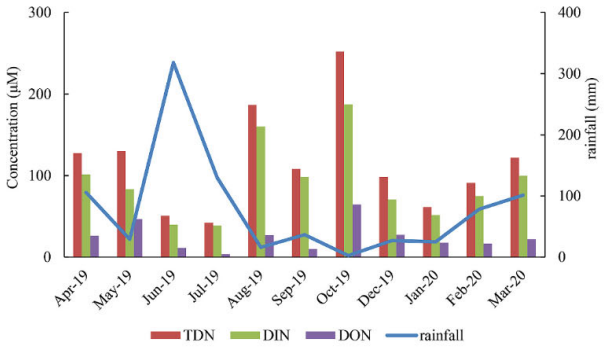

Fig. 5. Variations in rainfall and monthly average concentrations of TDN, DIN and DON in wet deposition.

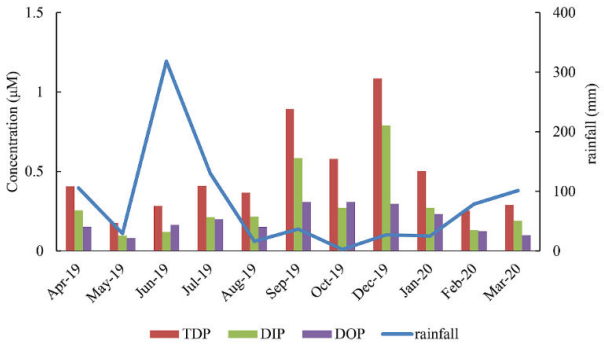

Fig. 6. Variations in rainfall and monthly average concentrations of TDP, DIP and DOP in wet deposition.

Table 2
Monthly average concentrations of nitrogen and phosphorus species in wet deposition (μM).

	TDN	DON	DIN	NH_4^+	NO_3^-	TDP	DOP	DIP	Rainfall (mm)
Apr-19	127.3	26.3	101.1	44.4	56.5	0.41	0.15	0.25	105.6
May-19	129.8	46.7	83.1	38.1	44.8	0.18	0.08	0.10	29.2
Jun-19	50.6	10.9	39.7	11.6	27.9	0.28	0.16	0.12	318.1
Jul-19	42.0	3.41	38.6	15.1	23.2	0.41	0.20	0.21	129.8
Aug-19	186.6	26.6	160.0	50.3	108.9	0.37	0.15	0.22	16
Sep-19	108.1	9.89	98.3	28.8	69.0	0.89	0.31	0.58	36.6
Oct-19	251.9	64.5	187.4	68.8	118.3	0.58	0.31	0.27	2.5
Dec-19	98.1	27.3	70.8	19.9	50.6	1.09	0.30	0.79	27.1
Jan-20	61.2	17.9	51.5	22.1	29.3	0.50	0.23	0.27	25
Feb-20	91.0	16.3	74.6	39.7	34.7	0.25	0.12	0.13	78.5
Mar-20	121.8	21.9	99.9	46.5	53.0	0.29	0.10	0.19	101.3
Mean	115.3 ± 61.3	24.7 ± 17.5	52.3 ± 18.9	35.0 ± 17.3	56.0 ± 31.7	0.48 ± 0.28	0.19 ± 0.08	0.28 ± 0.21	79.1 ± 89.8

Table 3
Annual fluxes of nitrogen and phosphorus in global atmospheric dry and wet deposition (mmol m^{-2} yr^{-1}).

Place	WSTN	WSTP	TDN	TDP	WSTN + TDN	WSTP + TDP	Reference
Jiaozhou Bay	75.9	0.26	195	0.72	271	0.98	Xing et al. (2018); Xing et al. (2017)
Kofu	22.9	–	–	–	–	–	Matsumoto et al. (2014)
Keelung	61	–	–	–	–	–	Chen et al. (2010)
Donsha	50	–	–	–	–	–	Chen and Huang (2018)
Singapore	41.7	4.51	111	1.65	153	6.16	He et al. (2011)
Crete	45.1	0.69	22	0.82	67.1	1.51	Violaki et al. (2017); Violaki et al. (2010)
Levantine basin	–	0.8	–	–	–	–	Carbo et al. (2005)
Turkey	21.1	–	–	–	–	–	Nehir and Koçak (2018)
Miami	22	0.10	29	0.09	51	0.19	Zamora et al. (2013)
Puerto Rico	–	–	17	–	–	–	Gioda et al. (2011)
Barbados	8.9	0.11	9.34	0.09	18.2	0.20	Zamora et al. (2013)
East China Sea (south side)	41.9 ± 11.6	0.083 ± 0.006	57.3 ± 11.3	0.32 ± 0.04	99.2 ± 22.9	0.41 ± 0.04	This study

the Yellow Sea (0.72 mmol m^{-2} yr^{-1}; Xing et al., 2017), and Singapore (0.66 mmol m^{-2} yr^{-1}; He et al., 2011). The high TDP flux in the Mediterranean is due to the supply of dust particles from the desert areas of North Africa; that in the Yellow Sea is due to human activities; and that in Singapore is due to high rainfall. The annual TDP flux (0.32 ± 0.04 mmol m^{-2} yr^{-1}; Eq. (6)) in the study area means that it is an area with lower TDP flux. Compared with Miami and Barbados in the North Atlantic, although the total rainfall in the study area (approximately 1000 mm) is lower, the P concentration and flux are relatively high due to the influence of continental human activities (fossil fuel burning, biomass burning, etc.) carried by the monsoons in winter and spring (Xing et al., 2017).

3.3. Molar concentration ratios of N to P and the global flux model

3.4.1. The molar concentration ratio of N to P in dry deposition

In this study area, the molar concentration ratio of WSIN/WSIP was 443 ± 366 (Fig. 7). The results showed that WSIN/WSIP was approximately 100–800 from April to November, but WSIN/WSIP was >1000 and even reached 1522 from December to March of the following year. In the winter and spring, the northeast monsoon brings industrial and agricultural emissions derived from mainland China, which causes the N concentration to rise. In summer and autumn, the main air masses come from oceanic sources in the south, greatly reducing the N concentration and increasing WSIN/WSIP (Wu et al., 2018). Fig. 8 shows that WSIN/WSIP is mostly high in East Asia, such as Jiaozhou Bay in the Yellow Sea (1251) (Xing et al., 2018), Qinhuangdao (574) in the Bohai Sea (Yu et al., 2020), and Shengsi Islands (729) in the middle of the East China Sea (Zhang et al., 2007). The main reason for the high WSIN/WSIP on the mainland is the large amount of reactive N emitted by human activities (Xing et al., 2018), especially near the sampling points in the northern industrial zone. In contrast, WSIN/WSIP tends to decrease gradually to the south, e.g., from the study area (443) to Daya Bay (only 24.6) (Wu et al., 2018) and Singapore (only 14.5) (He et al., 2011). Chen and Huang (2018) indicated that the flux of N in Asia decreases as the distance from the mainland increases. Therefore, the N in East Asia is affected mainly by terrestrial materials and human activities.

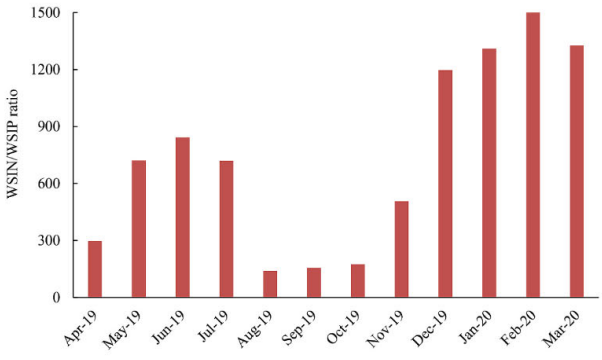

Fig. 7. Variations in the monthly average WSIN/WSIP ratio in dry deposition.

Zamora et al. (2013) pointed out that the main sources of P in Barbados and Miami in the North Atlantic are from North Africa (the Sahara Desert). Generally, the WSIN/WSIP ratio in Barbados is 234, but it drops to 179 during the sand and dust period; this ratio in Miami is 510 but falls to 453 during the sand and dust period. WSIN/WSIP tends to decrease during sandstorms because sand dust increases the concentration of P species, leading to a decrease in the ratio. However, Miami's WSIN/WSIP is higher than that in Barbados, mainly due to the difference in the N concentration. Since Miami is located in a densely populated area, its N emissions will be higher. Barbados, on the other hand, is an island that is far away from the mainland and therefore has lower N emissions. The WSIN/WSIP ratio in the study area (443) is similar to that in Miami because the two areas are both densely populated and are affected by anthropogenic active N emissions. Under these conditions, the concentration of N species is high, which leads to a higher WSIN/WSIP ratio.

The WSIN/WSIP ratio in Europe ranges from approximately 6.9 to 300, which is lower than that in this study and in other regions. The main reason for this difference is that southern Europe receives dust particles from the Sahara Desert; these particles are transported to the Mediterranean area by the monsoon and contain P (Violaki et al., 2017), resulting in low WSIN/WSIP ratios and even N restriction. For example, the WSIN/WSIP ratio of the Black Sea is 6.9 (Medinets and Medinets, 2012), and that of the Red Sea is 163 (Chen et al., 2007a,b). Since there were no dust storms in the study area during the sampling period, the P concentration was relatively low, at almost half of that in Europe.

3.4.2. The molar concentration ratio of N to P in wet deposition

In the study area, the molar concentration ratio of DIN/DIP is 333 ± 362, which is not as high as that of dry deposition (Fig. 9). In May 2019 and December 2019, the highest value of 870 and the lowest value of 90 occurred, respectively. The DIN/DIP of wet deposition has no obvious seasonal trend and does not exhibit the same trends as that of dry deposition. This may be due to the lowest DIP concentration occurring in May (0.10 μM) and the highest DIP concentration occurring in December (0.79 μM).

The distribution of the DIN/DIP ratio of wet deposition in Asia is similar to that of dry deposition (Fig. 10), and both decrease from north to south. The exceptions are the values of 37 in Kyushu and 24 in Hokkaido, Japan (Masaaki, 2020), which are low values for East Asia. The DIN/DIP ratios from north to south ranged from 832 on Shengsi Island in the East China Sea (Zhang et al., 2007) to 333 in the study area and 114 in Singapore (He et al., 2011). The ratios of N to P in the surface waters of the East China Sea and the Yellow Sea are 71.6 and 11.8, respectively; the wet deposition ratios are 333 (this study) and 533 (Xing et al., 2017), respectively, which are significantly higher. Therefore, the

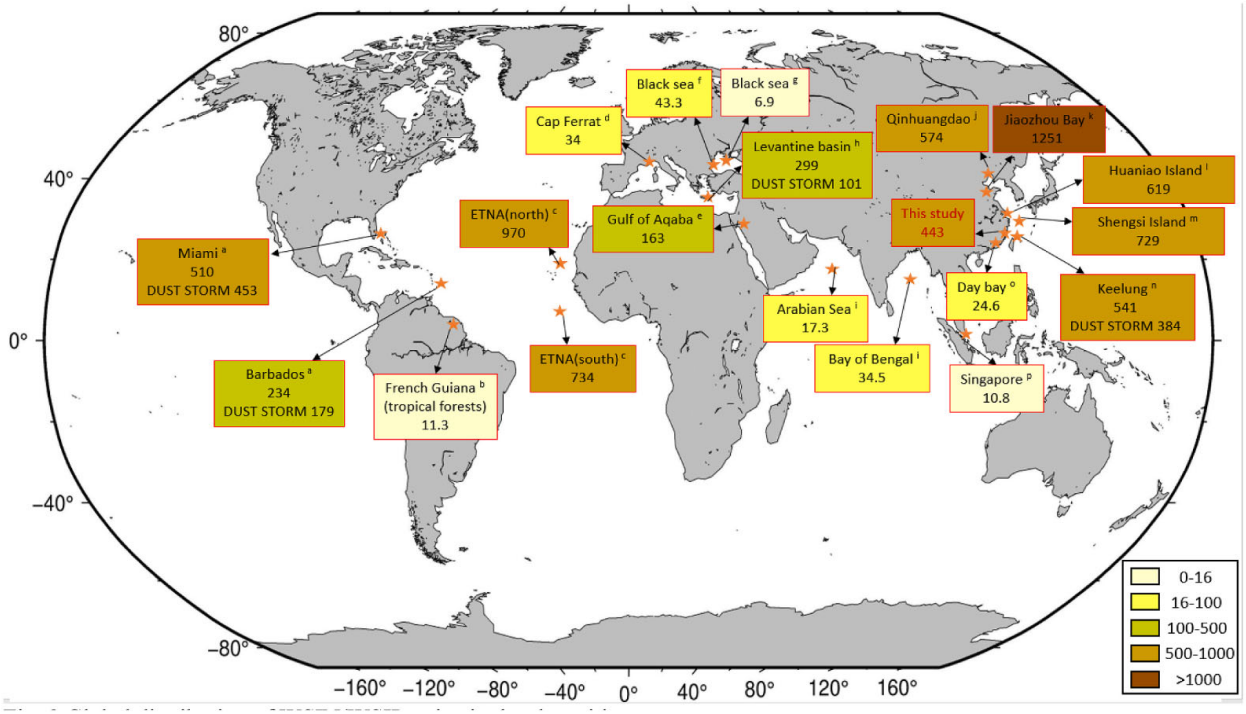

Fig. 8. Global distribution of WSIN/WSIP ratios in dry deposition. Note: [a]Zamora et al. (2013) [b]Van Langenhove et al. (2020) [c]Powell et al. (2015) [d]de Fommervault et al. (2015) eChen et al. (2007) [f]Koçak et al. (2016) [g]Medinets and Medinets (2012) [h]Carbo et al. (2005) [i]Srinivas and Sarin (2013) [j]Yu et al. (2020) [k]Xing et al. (2018) [l]Zhu et al. (2013) [m]Zhang et al. (2007) [n]Chen and Chen. (2008) [o]Wu et al. (2018) [p]Sundarambal et al. (2009).

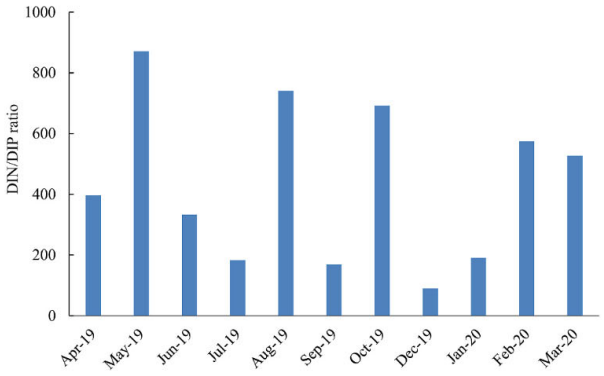

Fig. 9. Variations in the monthly average DIN/DIP ratio in wet deposition.

nutrients input by atmospheric wet deposition can alleviate the local N limitation and promote the growth of plankton (Zhang et al., 2007).

3.4.3. ON/OP ratio distribution in both dry and wet deposition

In dry deposition, the average WSON/WSOP is 327 ± 170, and the ratios of coarse and fine particles are 316 ± 367 and 333 ± 251, respectively. During the sampling period, the maximum ratio of WSON/WSOP occurred in February (1573), the minimum ratio occurred in September (106); the ratio between January and March was higher than 1000 (Fig. 11). These seasonal patterns occur because suspended particles of organic pollutants (N heterocyclic compounds, etc.) with high WSON concentrations are transported from mainland China in winter and spring; in contrast, in summer and autumn, sea salt from the south is the main source of WSON, and the concentration is relatively low (Wu et al., 2018). The WSON/WSOP ratios in this study are higher than those in Qinhuangdao (171) in the Yellow Sea (Yu et al., 2020), Jiaozhou Bay (440) in the Huanghai Sea (Xing et al., 2018), Daya Bay (54.4) in the northern part of the South China Sea (Wu et al., 2018) and Singapore (3.4) (He et al., 2011).

The average ratio of DON/DOP in wet deposition is 118 ± 132, with a maximum value of 577 and a minimum value of 17 in May and July, respectively (Fig. 12). The reason for the nearly 35-fold difference in DON/DOP may be the amount of rainfall. The low rainfall in May (29 mm) leads to a higher DON concentration (46.7 μM), while the higher rainfall in July (130 mm) causes dilution and a low DON concentration (3.41 μM). The DON/DOP values in different regions ranges from 35 in Miami in the southwestern North Atlantic (Zamora et al., 2013) to 105 in Jiaozhou Bay in the Huanghai Sea (Xing et al., 2017) and 16 in Singapore (He et al., 2011). Despite the low rainfall in the Yellow Sea (800 mm), the DON/DOP ratio in the study is similar; the DON/DOP in the study area is higher than that in other regions, which may be due to the low annual rainfall (1000 mm) during the sampling period. The DON/DOP ratio in this study is similar to that in the Yellow Sea, which experiences low rainfall (800 mm). This study is higher than that of other regions, which may be due to the low annual rainfall (1000 mm) during the sampling period in this study.

In this study, the ON/OP ratio of dry sedimentation (327 ± 170) is greater than the ON/OP ratio of wet sedimentation (118 ± 132). In winter and spring, dry deposition is influenced by the high concentrations of organic N pollutants released by mainland China, which increases the concentration of organic N (Wu et al., 2018) and therefore the ON/OP ratio. However, the ON/OP ratio of wet deposition is affected mainly by rainfall events, and the ratio is therefore lower in months with higher rainfall.

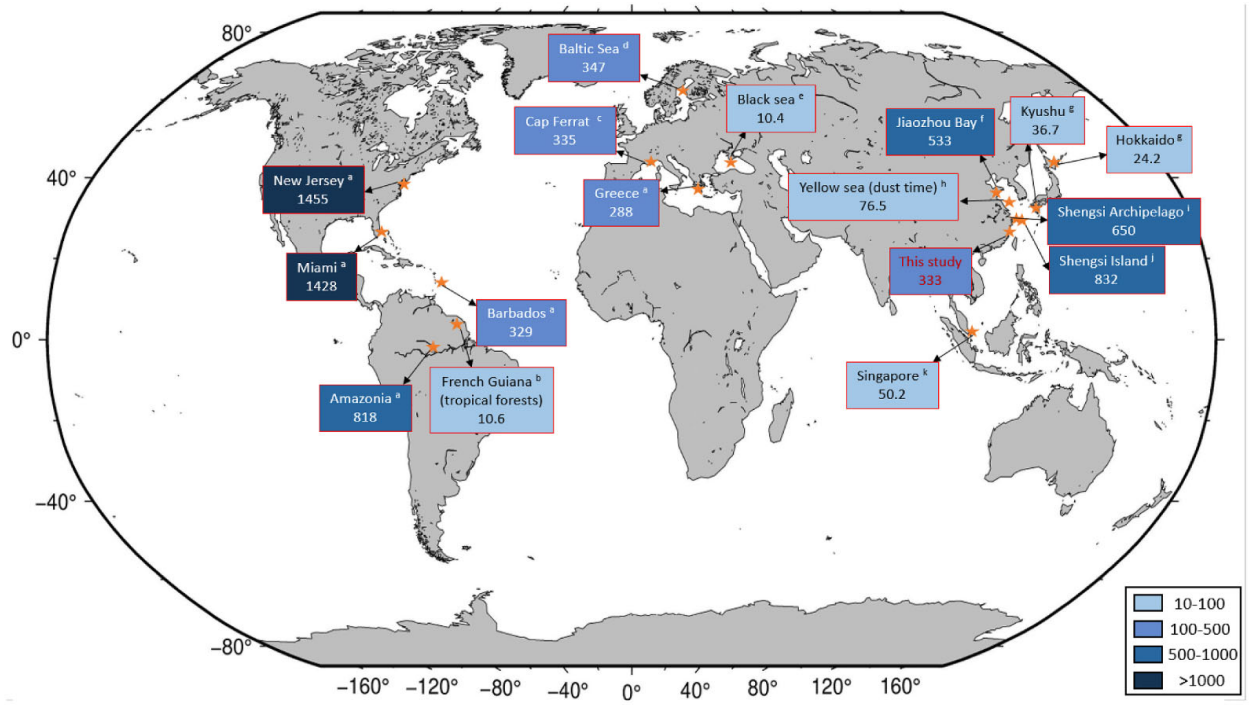

Fig. 10. Global distribution of the DIN/DIP ratio in wet deposition. Note: [a]Zamora et al. (2013) [b]Van Langenhove et al. (2020) [c]de Fommervault et al. (2015) [d]Rolff et al. (2008) [e]Medinets and Medinets (2012) [f]Xing et al. (2017) [g]Masaaki (2020) [h]Shi et al. (2013) [i]Zhu and Liu (2011) [j]Zhang et al. (2007) [k]He et al. (2011).

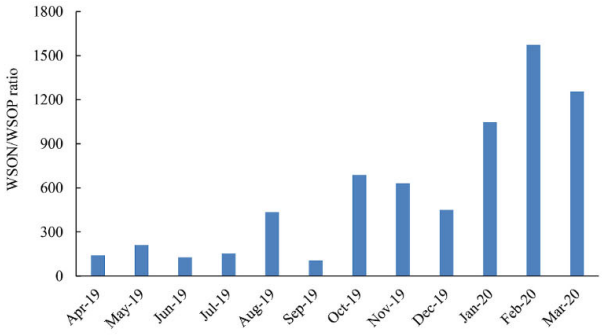

Fig. 11. Variations in the monthly average WSON/WSOP ratio in dry deposition.

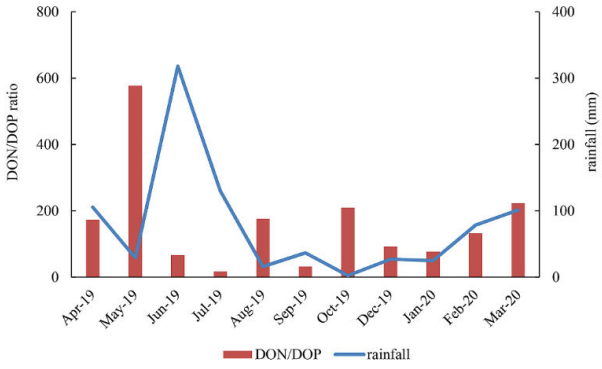

Fig. 12. Variations in the monthly average DON/DOP ratio in wet deposition.

3.4.4. G/M ratios estimated by the total N and total P flux model

The N deposition flux model of Galloway et al. (2008) found that three hotspots, East Asia, eastern North America, and western Europe, have relatively high N fluxes, at >1000 mg N m^{-2} yr^{-1}. Therefore, in this study, areas with N fluxes >1000 mg N m^{-2} yr^{-1} are regarded as high N flux areas, and other areas are considered low N flux areas. Mahowald et al. (2008) pointed out that the P fluxes near desert areas (North Africa, the Middle East and Northwest China) are usually relatively high. The P fluxes in regions affected by deserts are all >50 mg P m^{-2} yr^{-1}, so this study regards areas with >50 mg P m^{-2} yr^{-1} as high P flux deposition areas. All other areas are considered the low P flux areas. According to the above high- and low-flux classification system, the global N and P fluxes can be divided into areas with high N and high P (HNHP), high N and low P (HNLP), low N and high P (LNHP) and low N and low P (LNLP).

Fig. 13 shows that Western Europe is an HNHP area, which is due mainly to the high N flux (300–3000 mg N m^{-2} yr^{-1}) generated by human activities. Based on this, the estimated G/M ratio is approximately 900–2200. The Mediterranean area in southern Europe has a high P flux (5–100 mg P m^{-2} yr^{-1}) due to its proximity to the Sahara Desert, so its lowest ratio is approximately 30–150; this classifies it as LNHP (De Fommervault et al., 2015; Violaki et al., 2017). The southeastern coast of North America is an HNLP area. Due to the influence of human activities, the N flux in this area (300–2000 mg N m^{-2} yr^{-1}) is also high (Zamora et al., 2013). However, the flux of P species in this area (approximately 0.5–5 mg P m^{-2} yr^{-1}) is low, so the maximum G/M ratio (Eq. (7)) is approximately 1100–4400. The inland area of the United States (the west) is less affected by human activities than other areas of the United States, so the N flux is approximately 100–300 mg N m^{-2} yr^{-1}; this brings the G/M ratio to less than 110–450, indicating that this is an LNLP area.

The N flux in northern (inland) South America is approximately 100–1000 mg N m^{-2} yr^{-1}, and monsoon activity brings aerosols from this area to the Sahara Desert. Therefore, this area has a high P flux of

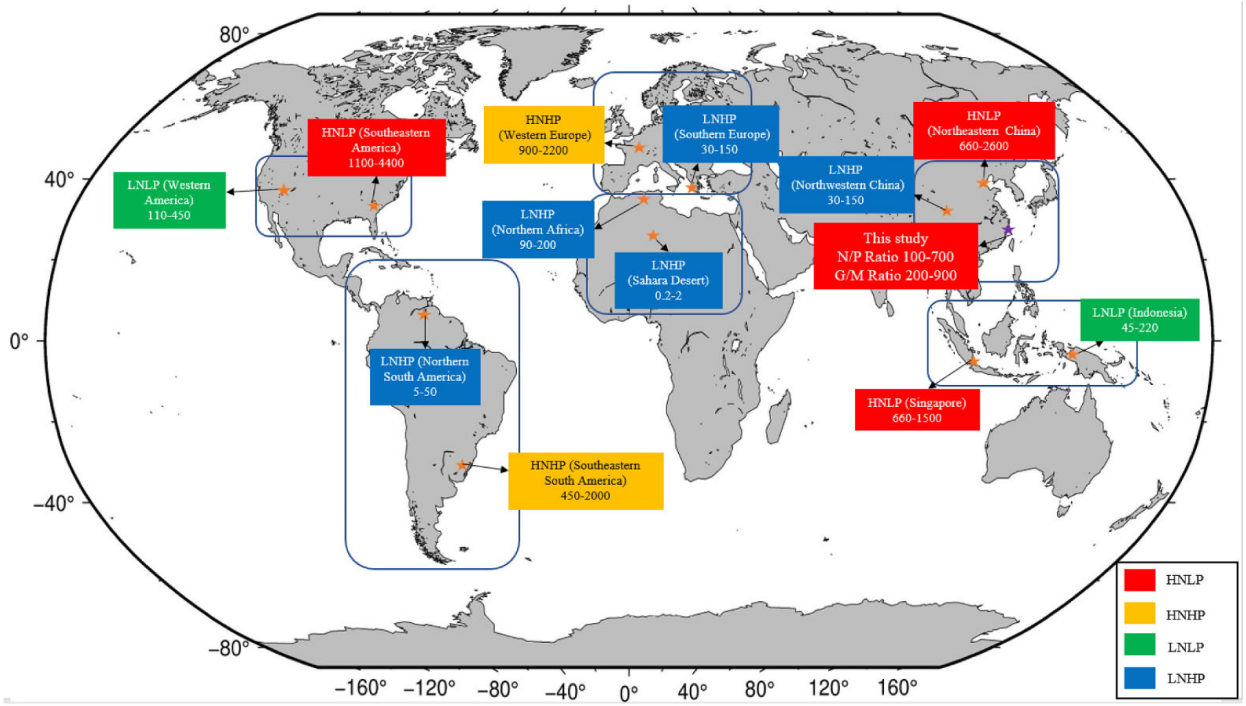

Fig. 13. Distribution of G/M ratios in atmospheric deposition in various regions of the world.

2–50 mg P m^{-2} yr^{-1} and the lowest G/M ratio detected in this study, 5–50. This area is an LNHP area (Zamora et al., 2013). The southeastern coast of Central and South America is densely populated and has the highest G/M ratio detected in this study, at 450–2000, indicating that it is an area of HNLP. The N flux in North Africa is only 50–500 mg N m^{-2} yr^{-1}; because this area includes the world's largest, the Sahara Desert, the P flux is the world's largest, at 10–500 mg P m^{-2} yr^{-1}. The highest G/M ratio (Eq. (7)) in this region occurs in the northern part of North Africa, at approximately 90–200, while the lowest G/M ratio occurs in the Sahara Desert (inland), at only 0.2–2 (Mahowald et al., 2008).

Southeast Asia is less affected by N emissions from human activities than other regions, and most parts of this area experience lower N and P fluxes (100–1000 mg N m^{-2} yr^{-1} and 0.5–5 mg P m^{-2} yr^{-1}, respectively). The minimum G/M ratio (Eq. (7)) in this region occurs in Indonesia, at approximately 45–220; this area is considered an LNLP area. In contrast, Singapore, which is densely populated, has a higher G/M ratio of approximately 660–1500, indicating that it is an HNLP area (Zamora et al., 2013; Shi et al., 2013). Due to the dense population in the coastal areas, Northeast Asia has the highest N flux (600–6000 mg N m^{-2} yr^{-1}) in the world, and the P flux is approximately 2–10 mg P m^{-2} yr^{-1}. Therefore, this area has the highest G/M ratio in East Asia, at approximately 660–2600, indicating that it is an HNLP area (Zhu et al., 2016). Since inland Northeast Asia has a relatively high P flux, at approximately 10–50 mg P m^{-2} yr^{-1}, Northwest China (inland) has a lower G/M ratio, of approximately 30–150. Therefore, it is an LNHP area.

The N and P fluxes determined from the two types of samples taken at the sampling site in this study are 1000–2000 mg N m^{-2} yr^{-1} and 5–10 mg P m^{-2} yr^{-1}, respectively, and the estimated G/M ratio range is 200–900. This result is in line with the nitrogen-to-phosphorus ratios (100–700) measured in this study, so the study area is an HNLP area. However, the G/M ratio (Eq. (7)) in the study area is lower than that in Northeast China (600–2600); this is because the N flux in Northeast Asia decreases from north to south (Chen and Huang. 2018). The N flux in northern China is significantly higher than that in southern China, and the study area is located in southeastern China at a certain distance from the area of high N emissions in northern China; as a result, the nitrogen-to-phosphorus ratios in the study area are lower.

4. Conclusion

Since the sampling site is close to mainland China, when seasonal winds come from the mainland in spring and winter, a higher concentration of WSTN is present in the dry deposition. Among N species, the proportion of NH_4^+ (89.1 ± 37.0 nmol m^{-3}) in WSIN was the highest. In terms of wet deposition, the concentration of TDN is composed mainly of NO_3^- (56.0 ± 30.2 μM), and the change in the TDN concentration is easily affected by the amount of rainfall. In terms of the total atmospheric flux, WSTN and TDN accounted for 42% (41.9 ± 11.6 mmol m^{-2} yr^{-1}) and 58% (57.3 ± 11.3 mmol m^{-2} yr^{-1}) of the total N flux, respectively. The results of this study show that wet deposition is the main contributor of N species, but the contribution ratio of WSTN to TDN is approximately 4:6. For P species, the WSTP concentration in dry deposition is composed of, in decreasing order, WSIP (0.35 ± 0.27 nmol m^{-3})> WSOP (0.16 ± 0.10 nmol m^{-3}), and the TDP concentration in wet deposition is composed of, in decreasing order, DIP (0.28 ± 0.20 μM)> DOP (0.20 ± 0.08 μM). WSTP and TDP accounted for 20% (82.6 ± 5.51 μmol m^{-2} yr^{-1}) and 80% (324 ± 37 μmol m^{-2} yr^{-1}) of the total P flux, respectively. These results show that wet deposition is also the main contributor of P species.

In this study, the average WSIN/WSIP is 443 ± 366, with relatively high ratios between December and March (both >1000). This result is consistent with the distribution of N species concentrations. The northeast monsoon is affected by the anthropogenic release of active N from the mainland, while the concentration of P has a tendency to decrease. In summer and autumn, the main wind direction changes to that of the southwest monsoon, this comes mostly from the sea.

Therefore, the concentrations of N species decrease, which in turn leads to a decrease in WSIN/WSIP (100–800). The DIN/DIP ratio is 333 ± 362; the maximum ratio (870) occurs in May, and the minimum ratio (90) occurs in December. The WSIN/WSIP (443 ± 366) and DIN/DIP (333 ± 362) ratios are approximately 5 times higher than that in the adjacent East China Sea (71.6). The high nitrogen-to-phosphorus ratios in the atmosphere in the study area may increase the P limitation of the surface seawater in the local waters (the East China Sea). The WSON/WSOP ratio of water-soluble organic species in atmospheric deposition is 327 ± 170, and the ratio is higher in winter than in spring. The distribution of the DON/DOP ratio (118 ± 132) in dissolved organic species is affected mainly by rainfall. The ratio is significantly lower in months with high rainfall and higher in months with low rainfall.

According to the global N and P model, this study divided the global distribution of N and P into four N and P distribution areas: HNHP, HNLP, LNHP, and LNLP areas. HNHP and HNLP areas are mainly located in densely populated areas and have high G/M ratios (450–4400). LNHP and LNLP are mostly located in inland or sparsely populated areas and have low G/M ratios (0.2–450). In densely populated areas, N fluxes are usually higher, which leads to an increase in the G/M ratio. Inland or desert-adjacent areas often have higher P fluxes or lower N fluxes, resulting in lower G/M ratios. Due to the lack of P inputs, the G/M ratio of coastal areas is higher than that of inland areas.

The N and P fluxes calculated by the global N and P model at the study site were 1000–2000 mg N m^{-2} yr^{-1} and 5–10 mg P m^{-2} yr^{-1}, respectively. Therefore, it is estimated that the G/M ratio range at the study site is approximately 200–900. This result is similar to the measured ratio obtained in this study (100–700). In addition, the ratio of N to P in East Asia tends to decrease from north to south, and the N flux in northern China is obviously higher than that in southern China. The study area is located in southeastern China and is a certain distance from the area of high N flux emissions in northern China; therefore, its G/M ratio is relatively low. However, the areas that are considered HNLP areas in this study are located mostly in densely populated areas near the sea (coastal China and the southeastern coast of the United States); this result highlights the problem of the imbalance in the nitrogen-to-phosphorus ratio caused by excessive active N emissions from human activities.

Declaration of competing interest

The authors declare that they have no known competing financial interests or personal relationships that could have appeared to influence the work reported in this paper.

Acknowledgments

The Ministry of Science and Technology of the Republic of China (grant MOST 110-2611-M-019-015) is acknowledged for the financial support.

References

Baker, A.R., Kelly, S.D., Biswas, K.F., Witt, M., Jickells, T.D., 2003. Atmospheric deposition of nutrients to the Atlantic Ocean. Geophys. Res. Lett. 30 (24), 2296.

Carbo, P., Krom, M.D., Homoky, W.B., Benning, L.G., Herut, B., 2005. Impact of atmospheric deposition on N and P geochemistry in the southeastern Levantine basin. Deep-Sea Res. II 52, 3041–3053.

Chen, H.Y., Chen, L.D., 2008. Importance of anthropogenic inputs and continental-derived dust for the distribution and flux of water-soluble nitrogen and phosphorus species in aerosol within the atmosphere over the East China Sea. J. Geophys. Res.: Atmosphere 113.

Chen, H.Y., Chen, L.D., Chiang, Z.Y., Hung, C.C., Lin, F.J., Chou, W.C., Gong, G.C., Wen, L.S., 2010. Size fractionation and molecular composition of water-soluble inorganic and organic nitrogen in aerosols of a coastal environment. 2010. J. Geophys. Res.: Atmosphere 115, D22307.

Chen, H.Y., Huang, S.Z., 2018. Effects of atmospheric dry deposition on external nitrogen supply and new production in the northern South China sea. Atmosphere 9 (10), 386.

Chen, H.Y., Huang, S.Z., 2020. Composition and supply of inorganic and organic nitrogen species in dry and wet atmospheric deposition: use of organic nitrogen composition to calculate the Ocean's external nitrogen flux from the atmosphere. Continent. Shelf Res. 213, 104316.

Chen, L.Y., Li, P., Yang, Y.H., 2016. Dynamic patterns of nitrogen: phosphorus ratios in forest soils of China under changing environment. J. Geophys. Res.: Biogeosciences 121, 2410–2421.

Chen, Y., Mills, S., Street, J., Golan, D., Post, A., 2007a. Estimates of atmospheric dry deposition and associated input of nutrients to Gulf of Aqaba seawater. J. Geophys. Res.: Atmospheres 112, D04309.

Chen, Y.X., Chen, H.Y., Wang, W., Yeh, J.X., Chou, W.C., Gong, G.C., Tsai, F.J., Huang, S. J., Lin, C.T., 2015. Dissolved organic nitrogen in wet deposition in a coastal city (Keelung) of the southern East China Sea: origin, molecular composition and flux. Atmos. Environ. 112, 20–31.

Chen, Y., Mills, S., Street, J., Golan, D., Post, A., Jacobson, M., Paytan, A., 2007b. Estimates of atmospheric dry deposition and associated input of nutrients to Gulf of Aqaba seawater. J. Geophys. Res. 112 (D4).

De Baar, H.J.W., 1994. von Liebig's law of the minimum and plankton ecology (1899-1991). Prog. Oceanogr. 33, 347–386.

De Fommervault, O.P., Migon, C., Dufour, A., D'Ortenzio, F., Kessouri, F., Raimbault, P., Garcia, N., Lagadec, V., 2015. Atmospheric input of inorganic nitrogen and phosphorus to the Ligurian Sea: data from the Cap Ferrat coastal time-series station. Deep Sea Res. Oceanogr. Res. Pap. 106, 116–125.

Elser, J.J., Bracken, M.E.S., Cleland, E.E., Gruner, D.S., Harpole, W.S., Hillebrand, H., Ngai, J.T., Seabloom, E.W., Shurin, J.B., Smith, J.E., 2007. Global analysis of nitrogen and phosphorus limitation of primary producers in freshwater, marine and terrestrial ecosystems. Ecol. Lett. 10, 1135–1142.

Fowler, D., Coyle, M., Skiba, U., Sutton, M.A., Cape, J.N., Reis, S., Sheppard, L.J., Jenkins, A., Grizzetti, B., Galloway, J.N., Vitousek, P., Leach, A., Bouwman, A.F., Butterbach-Bahl, K., Dentener, F., Stevenson, D., Amann, M., Voss, M., 2013. The global nitrogen cycle in the twenty-first century. Phil. Trans. Biol. Sci. 368 (1621).

Galloway, J.N., Townsend, A.R., Erisman, J.W., Bekunda, M., Cai, Z., Freney, J.R., Martinelli, L.A., Seitzinger, S.P., Sutton, M.A., 2008. Transformation of the nitrogen cycle: recent trends, questions, and potential solutions. Science 320 (5878), 889–892.

Garcia, C.A., Baer, S.E., Barcia, N.S., Rauschenberg, S., Twining, B.S., Lomas, M.W., Martiny, A.C., 2018. Nutrient supply controls particulate elemental concentrations and ratios in the low latitude eastern Indian Ocean. Nat. Commun. 9, 4868.

Gioda, A., Reyes-Rodríguez, G.J., Santos-Figueroa, G., Collett Jr., J.L., Decesari, S., Ramos, M.d.C.K.V., Netto, H.J.C.B., Neto, F.R.d.A., Mayol-Bracero, O.L., 2011. Speciation of water-soluble inorganic, organic, and total nitrogen in a background marine environment: cloud water, rainwater, and aerosol particles. J. Geophys. Res. 116, D05203.

He, J., Balasubramanian, R., Burger, D.F., Hicks, K., Kuylenstierna, J.C.I., Palani, S., 2011. Dry and wet atmospheric deposition of nitrogen and phosphorus in Singapore. Atmos. Environ. 45, 2760–2768.

Huang, X.L., Zhang, J.Z., 2009. Neutral persulfate digestion at sub-boiling temperature in an oven for total dissolved phosphorus determination in natural waters. Talanta 78 (3), 1129–1135.

Koçak, M., Mihalopoulos, N., Tutsak, E., Violaki, K., Theodosi, C., Zarmpas, P., Kalegeri, P., 2016. Atmospheric deposition of macronutrients (dissolved inorganic nitrogen and phosphorous) onto the Black Sea and implications on marine productivity. J. Atmos. Sci. 73, 1727–1739.

Mackey, K.R.M., Roberts, K., Lomas, M.W., Saito, M.A., Post, A.F., Paytan, A., 2012. Enhanced solubility and ecological impact of atmospheric phosphorus deposition upon extended seawater exposure. Environ. Sci. Technol. 46 (19), 10438–10446.

Mahowald, N., Jickells, T.D., Baker, A.R., Artaxo, P., Benitez-Nelson, C.R., Bergametti, G., Bond, T.C., Chen, Y., Cohen, D.D., Herut, B., Kubilay, N., Losno, R., Luo, C., Maenhaut, W., McGee, K.A., Okin, G.S., Siefert, R.L., Tsukuda, S., 2008. Global distribution of atmospheric phosphorus sources, concentrations and deposition rates, and anthropogenic impacts. Global Biogeochem. Cycles 22 (4), GB4026.

Martino, M., Hamilton, D., Baker, A.R., Jickells, T.D., Bromley, T., Nojiri, Y., Quack, B., Boyd, P., 2014. Western Pacific atmospheric nutrient deposition fluxes, their impact on surface ocean productivity. Global Biogeochem. Cycles 28 (7), 712–728.

Masaaki, C., 2020. Ten-year determination of atmospheric phosphorus deposition at three forested sites in Japan. Atmos. Environ. 223, 117247.

Matsumoto, K., Yamamoto, Y., Kobayashi, H., Kaneyasu, N., Nakano, T., 2014. Water-soluble organic nitrogen in the ambient aerosols and its contribution to the dry deposition of fixed nitrogen species in Japan. Atmos. Environ. 95, 334–343.

Medinets, S., Medinets, V., 2012. Investigations of atmospheric wet and dry nutrient deposition to marine surface in western part of the Black Sea. Turk. J. Fish. Aquat. Sci. 12, 497–505.

Mills, M.M., Ridame, C., Davey, M., Roche, J.L., Geider, R.J., 2004. Iron and phosphorus co-limit nitrogen fixation in the eastern tropical North Atlantic. Nature 429, 292–294.

Moore, C.M., Mills, M.M., Arrigo, K.R., Berman-Frank, I., Bopp, L., Boyd, P.W., Galbraith, E.D., Geider, R.J., Guieu, C., Jaccard, S.L., Jickells, T.D., La Roche, J., Lenton, T.M., Mahowald, N.M., Marañón, E., Marinov, I., Moore, J.K., Nakatsuka, T., Oschlies, A., Saito, M.A., Thingstad, T.F., Tsuda, A., Ulloa, O., 2013. Processes and patterns of oceanic nutrient limitation. Nat. Geosci. 6, 701–710.

Murphy, J., Riley, J.P., 1962. A modified single solution method for the determination of phosphate in natural waters. Anal. Chim. Acta 27, 31–36.

Nehir, M., Koçak, M., 2018. Atmospheric water-soluble organic nitrogen (WSON) in the eastern Mediterranean: origin and ramifications regarding marine productivity. Atmos. Chem. Phys. Discuss. 1–35.

Pai, S.C., Riley, J.P., 1994. Determination of nitrate in the presence of nitrite in natural waters by flow injection analysis with a non-quantitative on-line cadmium reductor. Int. J. Environ. Anal. Chem. 57 (4), 263–277.
Pai, S.C., Yang, C.C., 1990. Formation kinetics of the pink azo dye in the determination of nitrite in natural waters. Anal. Chim. Acta 232, 345–349.
Pai, S.C., Yang, C.C., Riley, J.P., 1990. Effects of acidity and molybdate concentration on the kinetics of the formation of the phosphoantimonylmolybdenum blue complex. Anal. Chim. Acta 229, 115–120.
Pai, S.C., Tsau, Y.J., Yang, T.I., 2001. pH and buffering capacity problems involved in the determination of ammonia in saline water using the indophenol blue spectrophotometric method. Anal. Chim. Acta 434 (2), 209–216.
Powell, C.F., Baker, A.R., Jickells, T.D., Bange, H.W., Chance, R.J., Yodle, C., 2015. Estimation of the atmospheric flux of nutrients and trace metals to the eastern tropical North Atlantic ocean. J. Atmos. Sci. 72 (10), 4029–4045.
Qi, J., Yu, Y., Yao, X., Gang, Y., Gao, H., 2020. Dry deposition fluxes of inorganic nitrogen and phosphorus in atmospheric aerosols over the Marginal Seas and Northwest Pacific. Atmos. Res. 245, 105076.
Rolff, C., Elmgren, R., Voss, M., 2008. Deposition of nitrogen and phosphorus on the Baltic Sea: seasonal patterns and nitrogen isotope composition. Biogeosciences 5, 1657–1667.
Shi, J.H., Zhang, J., Gao, H.W., Tan, S.C., Yao, X.H., Ren, J.L., 2013. Concentration, solubility and deposition flux of atmospheric particulate nutrients over the Yellow Sea. Deep Sea Res. Part II Top. Stud. Oceanogr. 97, 43–50.
Smil, V., 2000. Phosphorus in the environment: natural flows and human interferences. Annu. Rev. Energy Environ. 25, 53–88.
Spokes, L., Jickells, T., Weston, K., Gustafsson, B.G., Johnsson, M., Liljebladh, B., Conley, D., Skjøth, C.A., Brandt, J., Carstensen, J., Christiansen, T., Frohn, L., Geernaert, G., Hertel, O., Jensen, B., Lundsgaard, C., Markager, S., Martinsen, W., Møller, B., Pedersen, B., Sauerberg, K., Sorensen, L.L., Hasager, C.C., Sempreviva, A. M., Pryor, S.C., Lund, S.W., Larsen, S., Tjernstrøm, M., Svensson, G., Zagar, M., 2006. MEAD: an interdisciplinary study of the marine effects of atmospheric deposition in the Kattegat. Environ. Pollut. 140, 453–462.
Srinivas, B., Sarin, M.M., 2013. Atmospheric deposition of N, P and Fe to the northern Indian ocean: implications to C- and N-fixation. Sci. Total Environ. 456–457, 104–114.
Sundarambal, P., Balasubramanian, R., Tkalich, P., 2009. Atmospheric fluxes of nutrients onto Singapore Strait. Water Sci. Technol. 59 (11), 2287–2295.
Van Langenhove, L., Verryckt, L.T., Bréchet, L., Courtois, E.A., Stahl, C., Hofhansl, F., Bauters, M., Sardans, J., Boeckx, P., Fransen, E., Peñuelas, J., Janssens, I.A., 2020. Atmospheric deposition of elements and its relevance for nutrient budgets of tropical forests. Biogeochemistry 149, 175–193.
Violaki, K., Bourrin, F., Aubert, D., Kouvarakis, G., Delsaut, N., Mihalopoulos, N., 2017. Organic phosphorus in atmospheric deposition over the Mediterranean Sea: an important missing piece of the phosphorus cycle. Prog. Oceanogr. 163, 50–58.
Violaki, K., Zarbas, P., Mihalopoulos, N., 2010. Long-term measurements of dissolved organic nitrogen (DON) in atmospheric deposition in the Eastern Mediterranean: fluxes, origin and biogeochemical implications. Mar. Chem. 120 (1–4), 179–186.
Wu, Y.C., Zhang, J.P., Liu, S.L., Jiang, Z.J., Huang, X.P., 2018. Aerosol concentrations and atmospheric dry deposition fluxes of nutrients over Daya Bay, South China Sea. Mar. Pollut. Bull. 128, 106–114.
Xing, J., Song, J., Yuan, H., Wang, Q., Li, X., Li, N., Duan, L., Qu, B., 2018. Water soluble nitrogen and phosphorus in aerosols and dry deposition in Jiaozhou Bay, North China: deposition velocities, origins and biogeochemical implications. Atmos. Res. 207, 90–99.
Xing, J.W., Song, J.M., Yuan, H.M., Li, X.G., Li, N., Duan, L.Q., Kang, X.M., Wang, Q.D., 2017. Fluxes, seasonal patterns and sources of various nutrient species (nitrogen, phosphorus and silicon) in atmospheric wet deposition and their ecological effects on Jiaozhou Bay, North China. Sci. Total Environ. 576, 617–627.
Yan, G., Kim, G., 2015. Sources and fluxes of organic nitrogen in precipitation over the southern East Sea/Sea of Japan. Atmos. Chem. Phys. 15, 2761–2774. https://doi.org/10.5194/acp-15-2761-2015.
Yu, L., Ma, X., Gao, H., Zong, H., Yao, X., Lin, Z., Zhang, Z., Zhang, C., Yao, X., Zhang, Z., 2020. Distribution and source identification of nitrogen and phosphorus in aerosols in the Qinhuangdao coast, north China. Atmos. Environ. 234, 117475.
Zamora, L.M., Prospero, J.M., Hansell, D.A., Trapp, J.M., 2013. Atmospheric P deposition to the subtropical North Atlantic:sources, properties, and relationship to N deposition. J. Geophys. Res.: Atmospheres 118, 1546–1562.
Zhang, G.S., Zhang, J., Liu, S.M., 2007. Characterization of nutrients in the atmospheric wet and dry deposition observed at the two monitoring sites over Yellow Sea and East China Sea. J. Atmos. Chem. 57, 41–57.
Zhang, X., Lin, C., Zhou, X., Lei, K., Guo, B., Cao, Y., Lu, S., Liu, X., He, M., 2019. Concentrations, fluxes, and potential sources of nitrogen and phosphorus species in atmospheric wet deposition of the Lake Quinghai watershed, China. Sci. Total Environ. 682, 523–530.
Zhu, J., Wang, Q., He, N., Smith, M.D., Elser, J.J., Du, J., Yuan, G., Yu, G., Yu, Q., 2016. Imbalanced atmospheric nitrogen and phosphorus depositions in China: implications for nutrient limitation. J. Geophys. Res.: Biogeosciences 121 (6), 1605–1616.
Zhu, L., Chen, Y., Guo, L., Wang, F., 2013. Estimate of dry deposition fluxes of nutrients over the East China Sea: the implication of aerosol ammonium to non-sea-salt sulfate ratio to nutrient deposition of coastal oceans. Atmos. Environ. 69, 131–138.
Zhu, Y.M., Liu, S.M., 2011. Nutrients in atmospheric wet deposition in the East China Sea. Huanjing Kexue 32 (9), 2724–2731.